Chinese Journal of Polymer Science Vol. 34, No. 4, (2016), 505−512

Chinese Journal of Polymer Science

A Deblurring Procedure for Two-dimensional Small Angle X-ray Scattering Patterns*

Ran Chen[a], Zhi-yong Yi[a], Jia-xue Liu[a], Zhen-yu Liu[b**] and Yong-feng Men[a**]
[a] *State Key Laboratory of Polymer Physics and Chemistry, Changchun Institute of Applied Chemistry, Chinese Academy of Sciences, Changchun 130022, China*
[b] *Changchun Institute of Optics, Fine Mechanics and Physics, Chinese Academy of Sciences, Changchun 130033, China*

Abstract A general pre-processing procedure of the measured SAXS patterns for reducing the effect of beam stop and beam stop holder is described. A proper method for automatically choosing the regularization parameter is implemented. The method works out on the two-dimensional SAXS patterns. After deblurring, the corresponding two-dimensional patterns will be converted into one-dimensional integrated intensity distribution curves. We tested the program using both calculated artificial data and real experimental data such as polystyrene and poly(methyl methacrylate) latices. The deblurred results are satisfactory showing the effectiveness of the method. The deblurring process of a typical two-dimensional SAXS pattern using the Matlab based program can be completed in few seconds on normal personal computers.

Keywords: Deblur; PS latex; PMMA colloidal dispersion; SAXS.

INTRODUCTION

Small-angle X-ray scattering (SAXS) is a powerful tool for the investigation of structures of length scale from about several to hundreds of nanometers[1]. An ideal SAXS pattern should be generated from a high-intensity X-ray source with infinite small size. Due to finite direct-beam size and noise, the measured SAXS data always deviate from the ideal ones[2–4]. The most common solution is to balance the size and intensity of direct-beam to obtain scattering data with reasonable signal-to-noise ratio. In general, SAXS pattern is blurred by the direct-beam of finite dimension, especially for the ultra-SAXS (USAXS) experiments with long sample-to-detector distance and the occurrence of source divergence. A blurring effect will result in a significant deviation of measured data from the ideal scattering cross section making the data sometimes misleading. In such situation, blurring effect cannot be ignorable because systematic error could be produced in the data analysis. Therefore, it is necessary to deblur the measured SAXS patterns in order to acquire accurate results.

Several procedures have been proposed for the treatment of blurring effects in small-angle scattering. Guinier and Fournet[1] and DuMond[5] suggested an analytical solution for the experimental scattering curve in the case of infinite small slit-height beam. Modified versions of this approach have been developed by Schmidt[6], Schelten and Hossfeld[7] and others. Lake[8] developed an iterative procedure for the arbitrary height and width blurring. Glatter[9] modified this method by implicit smoothing technique to prevent the amplification of the statistical noise. Strobl[10] developed another desmearing method for any primary beam-intensity

---

* This work was financially supported by the National Natural Science Foundation of China (Nos. 21134006 and 51275504), Dutch Polymer Institute (DPI project: 779), and Science and Technology Development Plane of Jilin (No. 20140519007JH).
** Corresponding authors: Zhen-yu Liu (刘震宇), E-mail: liuzy@ciomp.ac.cn
Yong-feng Men (门永锋), E-mail: men@ciac.ac.cn
Received October 27, 2015; Revised November 21, 2015; Accepted November 22, 2015
doi: 10.1007/s10118-016-1767-7

distribution which can estimate the precision in the desmeared curve. The indirect Fourier transformation method was proposed for deblurring the experimental data by Glatter[11] and Moore[12]. This method finds the widest practical application but it needs a priori information about the object being investigated. Svergun[13] improved this method so that it did not require information about the range of definition of distance distribution function. Vonk[14] calculated the deblurred intensity values directly from a digitized expression by weighted least squares. Modified version of the method of Vonk[14] has been developed by Singh *et al*.[15] who made it efficient and stable in real application. Svergun *et al*.[16] applied the Tiknonov regularization method to solve the ill-posed problems in small-angle scattering data treatment including the slit-width and polychromaticity correction. Le Flanchec *et al*.[17] investigated the two-dimensional deblurring of centrosymmetric SAXS patterns after corrections of geometrical distortions and converting into polar coordinates. However, the problem of real two-dimensional (2D) deblurring of SAXS patterns still exists.

In this work, we investigate the application of the fast Fourier transform (FFT)-based Tikhonov regularization method, which was proposed in the image deblurring field by Hansen *et al*.[18], in treating SAXS patterns in reciprocal space. The most significant feature of this method is that it provides efficient calculation without constructing a large blurring matrix and ease of implementation. No more limitation is placed on beam pattern which can be arbitrary. In comparison with other methods in this field, measured data were directly utilized in the present method and no preceding smoothing procedures were needed. The method was tested by artificial and real experimental data showing that it is available for practical application.

METHOD

Deblurring Method

The fast Fourier transform (FFT)-based Tikhonov regularization method was suggested by Hansen *et al*[18]. The main blurring effect in SAXS arises from the size and intensity distribution of the direct beam. And the measured SAXS pattern is a convolution of the ideal pattern with blurring function. The goal of FFT-based Tikhonov regularization method is to reconstruct the ideal SAXS patterns and to infer the certain hidden data from the measured data on the basis of the recorded blurred SAXS patterns and the image of direct beam.

Let $\mathbf{X}\in \mathrm{R}^{m\times n}$ represent the desired sharp SAXS pattern, while $\mathbf{B}\in \mathrm{R}^{\mathrm{m}\times \mathrm{n}}$ represents the recorded blurred SAXS pattern. The general mathematical model for blurring process is

$$\mathbf{Ax} = \mathbf{b} \tag{1}$$

where $\mathbf{x}$ and $\mathbf{b}$ are two long vectors obtained by stacking the matrices of $\mathbf{X}$ and $\mathbf{B}$ into vectors, both of length $N = m \times n$. $\mathbf{A}\in \mathrm{R}^{N\times N}$ is the large blurring matrix which represents the blurring that is taking place in the process of going from the exact to the blurred image.

The blurring matrix $\mathbf{A}$ is determined by two ingredients: the point spread function (PSF) and the boundary condition. PSF defines how each pixel is blurred and can be obtained experimentally and analytically. Here we assume the image of direct-beam on the detector to be PSF, which is measured in the absence of samples and beam stop. The boundary condition is to assume the behavior of the ideal pattern outside the boundary, including zero, periodic and reflexive boundary conditions. For the periodic boundary condition, the blurring matrix is block circulant with circulant blocks (BCCB). BCCB matrix is normal so that the blurring matrix has the spectral decomposition

$$\mathbf{A} = \mathbf{F}^{*}\mathbf{\Lambda}\mathbf{F} \tag{2}$$

where $\mathbf{F}$ is the two-dimensional unitary discrete Fourier transform matrix. We can perform $\mathbf{F}$ and $\mathbf{F}^*$ computations efficiently by Matlab functions fft2 and ifft2 which support 2D fast Fourier transform and 2D inverse fast Fourier transform. Therefore, the eigenvalues of $\mathbf{A}$ can be computed efficiently using the FFT algorithm.

Usually $\mathbf{x} = \mathbf{A}^{-1}\mathbf{b}$ is not a good solution because the matrix $\mathbf{A}$ is severely ill-posed. At the same time, the inverted noise can dominate in the deblurred image. In order to diminish the effect of noise in $\mathbf{b}$, we filter the solution by Tikhonov regularization method. The filter factors are defined as

$$\Phi_i = \frac{\sigma_i^2}{\sigma_i^2 + \alpha^2}, \; i = 1, \ldots N \tag{3}$$

where $\alpha > 0$ is called the regularization parameter and σ_i is the eigenvalue of blurring matrix **A**. This choice of filter factors yields the solution vector $\mathbf{x}_\alpha$ for the minimization problem

$$\min_X \left\{ \|\mathbf{b} - \mathbf{AX}\|_2^2 + \alpha^2 \|\mathbf{x}\|_2^2 \right\} \tag{4}$$

where the regularization parameter α adjusts the weight to the minimization of the side constraint relative to the minimization of the residual norm.

Pre-processing Procedure

In the SAXS setup, there is a beam stop which is held by a wire in front of the detector to stop the incident beam. However, the wire will stop part of the scattered X-ray during the experiments. In this situation, the obtained SAXS patterns are incomplete. It is essential to solve this problem to avoid serious deviation in the deblurred patterns.

To eliminate the influence of metal wire, one could change the position of detector relative to the direct beam. Figure 1(a) shows a typical two-dimensional SAXS pattern of latex powders collected on a modified Xeuss system of Xenocs, France. The center of direct-beam is at the bottom of the detector. The pre-processing procedure about SAXS pattern is to mirror the pattern with respect to the horizontal axis passing through the beam center. The SAXS pattern in Fig. 1(b) shows the pre-processing result. However, the influence of beam stop cannot be removed after pre-processing. Thus, the second step is to extrapolate the scattering intensity toward beam center to prevent the occurrence of negative values in the pixels at the position of beam stop. A simple method is to set a proper value in beam stop area. In this way, there will be no negative data at beam stop position of deblurred pattern minimizing the deviation of the same position. For sake of simplicity, the value is defined as the average intensity on the edge of beam stop.

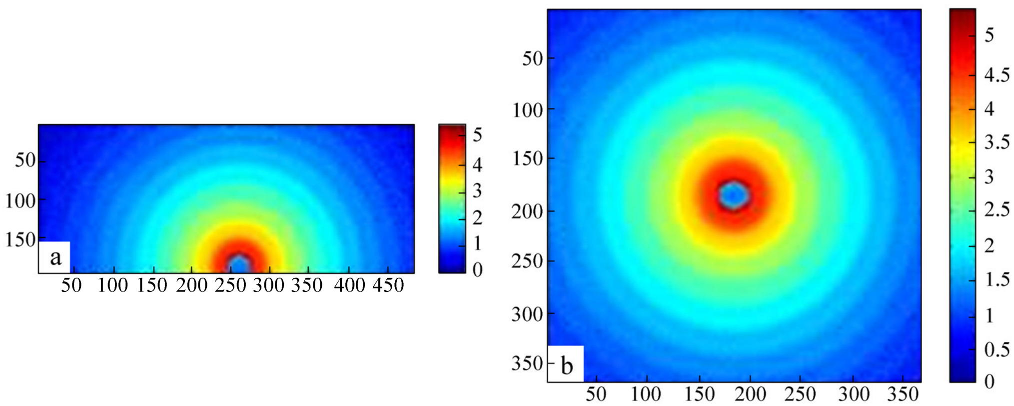

Fig. 1 (a) Typical SAXS pattern of latex powders on the modified Xeuss system of Xenocs, France (logarithmic beam intensity in linear plot); (b) The pre-processed SAXS pattern after mirroring the measured pattern with respect to the axis passing through beam center

The point spread function is represented as the image of direct beam on the detector. The image is measured without samples and beam stop within one second. Figure 2 shows a typical direct beam image. One observes clearly a square-shaped direct beam. In order to reduce the noise, only the data in the square-shaped direct beam area was chosen during the deblurring procedure. The point spread function was normalized with respect to the total intensity.

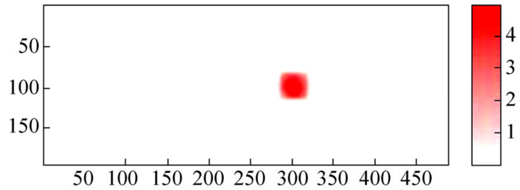

Fig. 2 Typical direct beam image measured in the absence of beam stop and sample (logarithmic beam intensity in linear plot)
Slit size is 1.0 mm × 1.0 mm (horizontal by vertical, respectively).

Parameter Choice Method

Constructing a proper method to choose the regularization parameter is an important issue for automatic application. The value provided by the generalized cross validation[18] (GCV) method is always so small that the solution is under-smoothing. To avoid under-smoothing, a method by controlling the pixel with negative value within a certain q range was utilized. The pixel with negative value occurs because of the reconstruction errors from data and rounding errors. Although the pixel with negative value has no physical meaning for SAXS patterns, it often happens in numerical computations. The real parts of DFT-based basis components for the filtered solution are images in which the pixels with positive and negative values alternate in different frequency. The low-frequency spectral components are needed to describe the main characteristics of the image, while the high-frequency spectral components are used to represent the details of the image. The magnitude of the high-frequency spectral components is usually smaller than that of the low-frequency components, so the high-frequency information is highly damped or even lost in the blurring process and it is easy to be contaminated by the noise. The general position of pixels with negative values in the deblurred scattering pattern for latex powders is shown in Fig. 3. The areas with red color represent pixels with negative values. The pixels with negative values always appear in the position where the signal is weak. We can choose the regularization parameter by controlling that there is no pixel with negative value in certain scatter vector area. With the normalization of the point spread function the largest eigenvalue of blurring matrix is 1, so that the regularization parameter is between 0 and 1. We use the bisection method with maximum to iterations to find a suitable regularization parameter. A large parameter ensures suppressing noise and has less pixels with negative values. However, it makes the deblurred patterns with over-smoothing effect. A small parameter means little filtering that leads to an under-smoothing reconstruction dominated by noise. And there are more pixels with negative values in this way. As the regularization parameter increases, the number of pixels with negative values and the degree of deblurring both decrease.

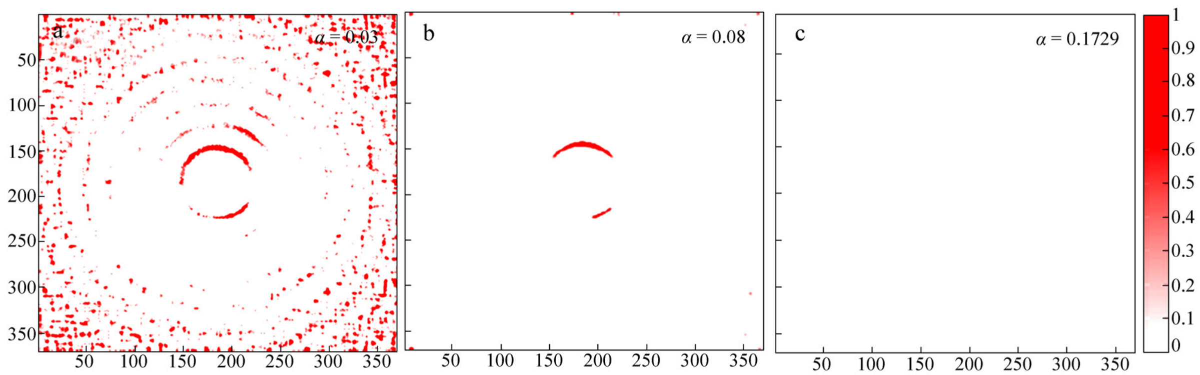

Fig. 3 The general position of the pixels with negative values in the deblurred pattern for latex powders under different regularization parameters (The red color area represents the pixels with negative values.)

RESULTS AND DISCUSSION

Applications to Artificial Data

This method is first applied to artificial data in order to illustrate the effect of deblurring with the known original data. The model is a homogeneous sphere of 80 nm in radius. The scattering curve of such sphere consists of a series of maxima and minima given by

$$I(q) \sim \left[3\frac{\sin(qR) - qR\cos(qR)}{(qR)^3} \right]^2 \tag{5}$$

where R is the radius of the homogeneous sphere, q is the scattering vector.

The blurred pattern I_{blur} is generated by convolution of model pattern with a 2D Gaussian function. The deviation of the Gaussian function is 6 pixels. It is necessary to include additional noise for the artificial calculated data. There are two ways to add noise. One is using a random-number generator[19] according to

$$\sigma(q) = \pm n_\sigma p I_{\text{blur}}(q) \tag{6}$$

where p is a random number describing the fraction of $n_\sigma I_{\text{blur}}(q)$ to be randomly added to or subtracted from the intensity value $\boldsymbol{I}_{\text{blur}}(q)$. The parameter n_σ corresponds to the maximum relative deviation and is set to value of 0.050. The other is to add Gaussian white noise[18]. For example, the ratio of the norm of noise to blurred pattern $\|\boldsymbol{e}\|_2/\|\boldsymbol{I}_{\text{blur}}\|_2$ is 0.001, meaning that 0.1% noise is added to the blurred data. And we add random perturbation to the blurred patterns by both ways, respectively.

In real experiment, beam stop is used to prevent direct beam from striking the detector. However, it leads to some scattering information lost. To make the artificial data close to the real experimental data, we deducted pixels in the central area of the patterns. The deducted area is $q < 0.015$ nm^{-1}. And a proper constant value is filled in the deducted area to see the difference in deblurred data.

Based on the first way of adding noise, the deblurred, model and blurred curves for different conditions are acquired as shown in Fig. 4. For noiseless data in Fig. 4(a), the method is almost able to restore the sharp minimum completely. Deblurring becomes much easier without noise. For noisy data ($n_\sigma = 0.050$), the deblurred result is fairly well. Only the very narrow feature cannot be restored wholly. This may be expected, since the detailed information is easy to be ruined by noise. Two sets of comparison are made. One is between Figs. 4(a) and 4(c), the other is between Figs. 4(b) and 4(d). One can observe that deducting the central area does not make much difference. It only leads to little deviation in the deducted area.

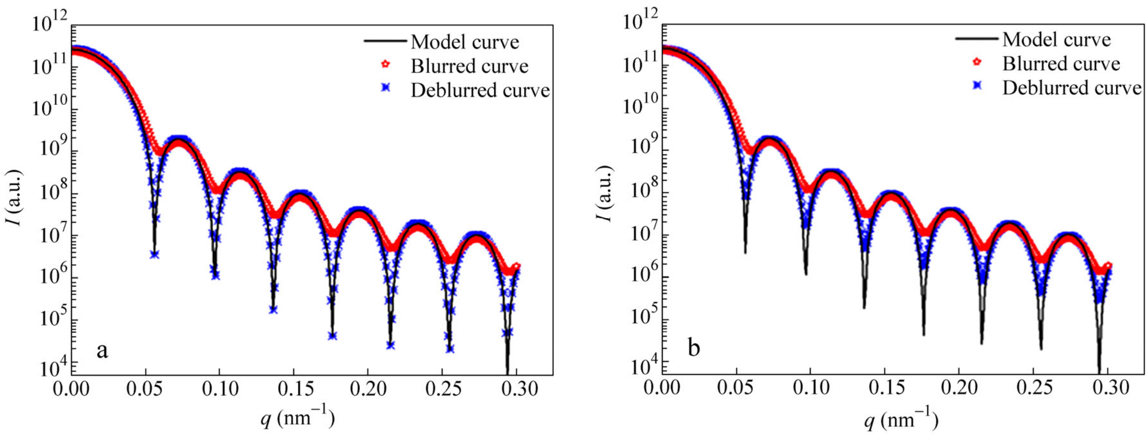

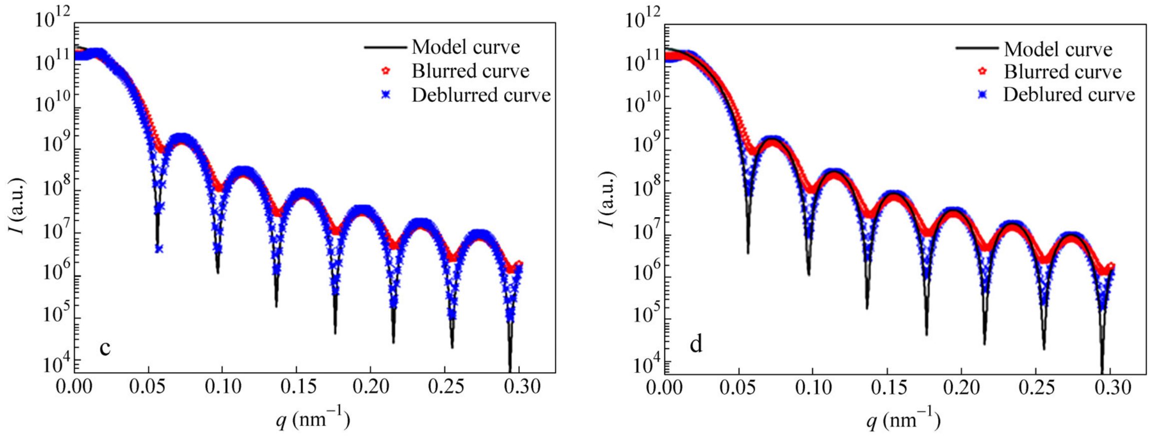

Fig. 4 Restoration of model scattering intensity of a homogeneous sphere blurred by Gaussian function for different noise levels n_σ and with or without deducting in the central area: (a) the noise level $n_\sigma = 0.000$ without deducting the central area, (b) the noise level $n_\sigma = 0.050$ without deducting the central area, (c) the noise level $n_\sigma = 0.000$ and the deducted area $q < 0.015$ nm^{-1} and (d) the noise level $n_\sigma = 0.050$ and the deducted area $q < 0.015$ nm^{-1}

For the second way of adding noise, the deblurred, model and blurred curves with or without deducting the central areas are shown in Fig. 5. The noise added in this way is Gaussian white noise with level of 0.1%. The noise in one pixel has no relation to the intensity in the same pixel. It leads to the fact that the percentage of noise in the sharp minimum position is much greater than that in other positions.

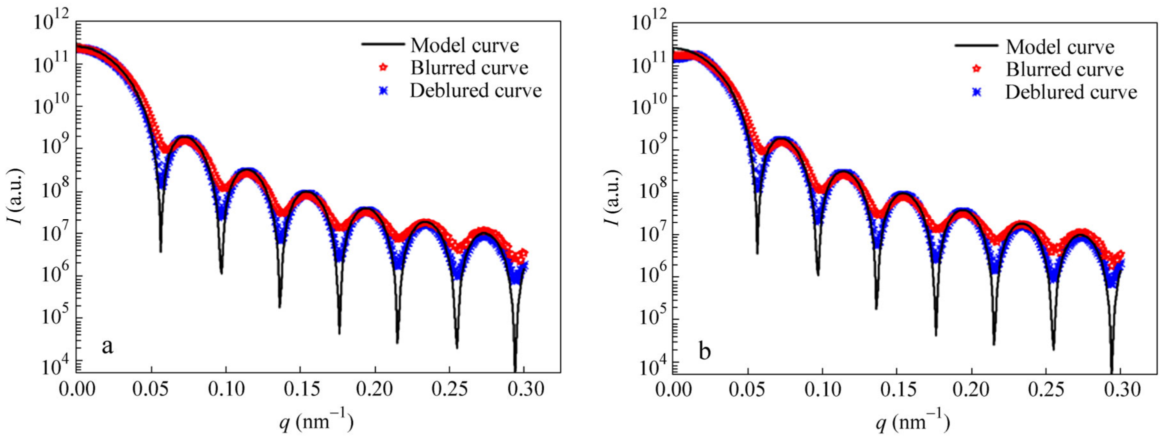

Fig. 5 Restoration of model scattering intensity of a homogeneous sphere blurred by Gaussian function: (a) without deducting the central area and (b) the deducted area $q < 0.015$ nm^{-1} (The noise level is 0.1%.)

Application to the Experimental Data

For the application of the deblurring procedures to the experimental data, two samples were chosen: one is polystyrene (PS) latex powders, the other is poly(methyl methacrylate) (PMMA) colloidal dispersion. They are both spherical in shape. SAXS experiments were carried out on a modified Xeuss system of Xenocs, (France) equipped with a semiconductor detector (Pilatus 100K, DECTRIS, Swiss) attached to a multilayer focused Cu Kα X-ray source (GeniX3D Cu ULD, Xenocs SA, France), generated at 50 kV and 0.6 mA. The wavelength of the X-ray radiation was 0.154 nm. The sample-to-detector distance was 6520 mm. The setup is equipped with two scatterless slits systems 2.4 meters apart from each other located in between the X-ray source and sample. The motor driven slits system can shape the incident X-ray beam into different sizes.

The noise in the SAXS patterns puts limit on the size of the details we hope to restore, *i.e.*, noise may lead to a permanent loss of some detailed information. However with the same noise level, the restoration degree should be the same. The polystyrene latex powders were measured with direct-beam of different slits sizes. The photon flux increased with increasing slits size of direct-beam. To keep the same noise level for the experiments of different slits sizes the exposure time was calculated using the photon flux at different slits sizes as present in Table 1.

Table 1. The exposure time for the sample of polystyrene latex powders

Slits opening (mm×mm)	1.0 × 1.0	0.9 × 0.9	0.8 × 0.8	0.7 × 0.7	0.6 × 0.6	0.5 × 0.5
Photon flux (counts·s^{-1})	20326	15083	10086	6326	3534	1663
Exposure time (s)	100	136	203	322	579	1241

After correcting for transmitted flux, background and exposure time, the SAXS patterns were averaged azimuthally. The 1D SAXS curves are shown in Fig. 6(a). It is clear that the blurring effect decreases with the decreasing in slit size. The maxima and minima in the observed scattering intensity distribution curve are more obvious when the slit sizes are small. After the deblurring process, the 1D averaging curves are shown in Fig. 6(b). The deblurred curves obtained under the condition of different silts sizes are almost the same. The deviation at small q range is caused by beam stop.

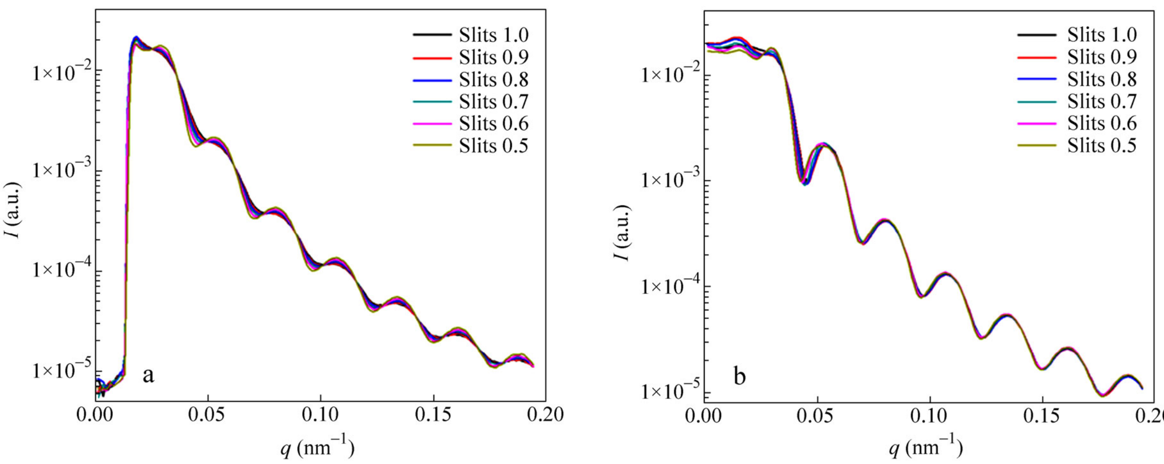

Fig. 6 (a) Experimental SAXS data of PS latex powders with different slits sizes of direct-beam; (b) Deblurred curves of the experimental data of PS latex powders in Fig. 6(a)

In the experiment of PMMA colloidal dispersion, the size of direct-beam slits was 0.7 mm × 0.7 mm and the exposure time was 7200 sec. Figure 7 (a) shows the non-linear least-squares fitting of blurred model to the experimental data. The obtained radius of colloid is 86.9 nm and the corresponding deviation is 3.2 nm. Figure 7(b) shows the comparison of deblurred data and the model fitted data. The deblurred data follow the model fitted data very well which indicates that the deblurring method is efficient. For comparison, the scattering curve without deblurring has also been used to calculate particle size and size distribution (data not shown). The thus obtained radius is 85.9 nm with a deviation of 5.3 nm. Obviously, these values deviate from the true values shown above. Therefore, in case of spherical latex particles, the size distribution obtained is not correct without deblurring. In order to control the size of latex particles in the synthetic process, it is essential to determine the true size distribution.

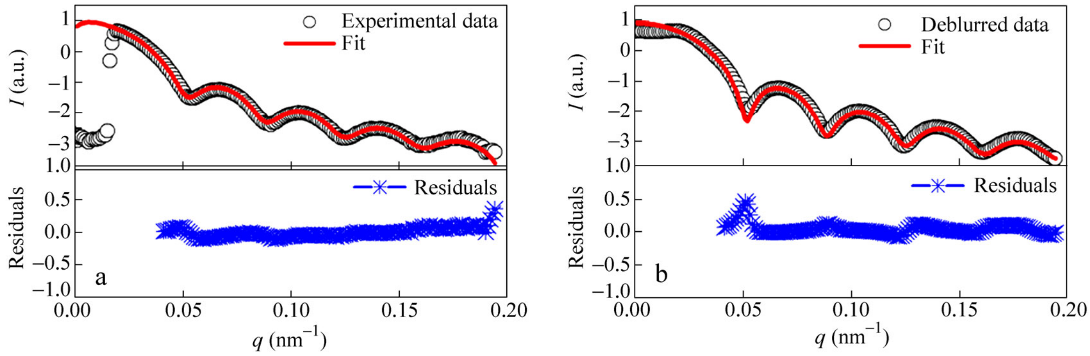

Fig. 7 (a) The non-linear least-squares fitting of blurred model to the experimental data (The obtained radius is 86.9 nm. Deviation is 3.2 nm. The smear width is 0.0044 nm^{-1}.); (b) The comparison of the deblurred data and the model fitted data

CONCLUSIONS

The FFT-based Tikhonov regularization method provides an excellent procedure for efficient correction of the beam-size blurring effect and is available for direct-beam of arbitrary shape. The measured direct-beam pattern can be used directly without any transformation or numerical interpolation. This method works out well on artificial patterns and experimental patterns. Excellent and useful results are given. Provided with the spectral factorization of the blurring matrix **A**, we can compute the filtered solution efficiently *via* the fast Fourier transform and with less demanding on memory of the computer. It does not need preliminary smoothing procedure. A Matlab program for this method used here can be obtained from the authors.

REFERENCES

1 Guinier, A. and Fournet, G., "Small-angle scattering of X-rays", John Wiley & Sons Inc, New York, 1955
2 Pedersen, J.S., Adv. Colloid Interface Sci., 1997, 70: 171
3 Register, R.A. and Cooper, S.L., J. Appl. Cryst., 1988, 21: 550
4 Kube, O. and Springer, J., J. Appl. Cryst., 1985, 18: 308
5 DuMond, J., Phys. Rev., 1947, 72(1): 83
6 Schmidt, P.W., Acta Crystallogr., 1965, 19(6): 938
7 Schelten, J. and Hossfeld, F., J. Appl. Cryst., 1971, 4(3): 210
8 Lake, J.A., Acta Crystallogr., 1967, 23(2): 191
9 Glatter, O., J. Appl. Cryst., 1974, 7(2): 147
10 Strobl, G.R., Acta Crystallogr., Sect. A: Found. Crystallogr., 1970, 26(3): 367
11 Glatter, O., J. Appl. Cryst., 1977, 10(5): 415
12 Moore, P.B., J. Appl. Cryst., 1980, 13(2): 168
13 Svergun, D.I., J. Appl. Cryst., 1993, 26(2): 258
14 Vonk, C.G., J. Appl. Cryst., 1971, 4(5): 340
15 Singh, M.A., Ghosh, S.S. and Shannon Jnr, R.F., J. Appl. Cryst., 1993, 26(6): 787
16 Svergun, D.I., Semenyuk, A.V. and Feigin, L.A., Acta Crystallogr., Sect. A: Found. Crystallogr., 1988, 44(3): 244
17 Le Flanchec, V., Gazeau, D., Taboury, J. and Zemb, T., J. Appl. Cryst., 1996, 29(2): 110
18 Hansen, P.C., Nagy, J.G. and O'Leary, D.P.,"Deblurring images: matrices, spectra, and filtering", SIAM, Philadelphia, 2006
19 Vad, T. and Sager, W.F.C., J. Appl. Cryst., 2011, 44(1): 32